

Quantum phase diagram of the generalized ionic Hubbard model for AB_n chains

M. E. Torio,¹ A. A. Aligia,² G. I. Japaridze,³ and B. Normand^{4,2}

¹*Instituto de Física Rosario, Consejo Nacional de Investigaciones, Científicas y Técnicas and Universidad Nacional de Rosario, Boulevard 27 de Febrero 210 Bis, 2000 Rosario, Argentina*

²*Centro Atómico Bariloche and Instituto Balseiro, Comisión Nacional de Energía Atómica, 8400 Bariloche, Argentina*

³*Institute of Physics, Georgian Academy of Sciences, Tamarashvili 6, 0177 Tbilisi, Georgia*

⁴*Département de Physique, Université de Fribourg, CH-1700, Fribourg, Switzerland*

We investigate the ground-state phase diagram of the Hubbard model for the AB_{N-1} chain with filling $1/N$, where N is the number of atoms per unit cell. In the strong-coupling limit, a charge transition takes place from a band insulator (BI) to a correlated insulator for increasing on-site repulsion U and positive on-site energy difference Δ (energy at A sites lower than at B sites). In the weak-coupling limit, a bosonization analysis suggests that for $N > 2$ the physics is qualitatively similar to the case $N=2$ which has already been studied: an intermediate phase emerges, which corresponds to a bond-ordered ferroelectric insulator (FI) with spontaneously broken inversion symmetry. We have determined the quantum phase diagram for the cases $N=3$ and $N=4$ from the crossings of energy levels of appropriate excited states, which correspond to jumps in the charge and spin Berry phases, and from the change of sign of the localization parameter z_L^c . From these techniques we find that, quantitatively, the BI and FI phases are broader for $N > 2$ than when $N=2$, in agreement with the bosonization analysis. Calculations of the Drude weight and z_L^c indicate that the system is insulating for all parameters, with the possible exception of the boundary between the BI and FI phases.

DOI: [10.1103/PhysRevB.73.115109](https://doi.org/10.1103/PhysRevB.73.115109)

PACS number(s): 71.10.Hf, 71.45.Lr, 78.20.Bh

I. INTRODUCTION

The half-filled Hubbard chain with alternating on-site energies $\pm\frac{1}{2}\Delta$, known as the ionic Hubbard model (IHM), was proposed^{1,2} to describe the neutral-ionic transition in mixed-stack charge-transfer organic crystals such as tetrathiafulvalene-*p*-chloranil.^{3,4} Interest in the model increased in the last decade due to its potential application to ferroelectric perovskites.⁵⁻¹² Although some details of the phase diagram, excitations, and expected physical properties of certain phases remain to be established, recent research has revealed the essential physics of the model.¹⁰⁻¹⁹

It is self-evident that in the limit of vanishing hopping, $t \rightarrow 0$, the ground state is a band insulator (BI) for on-site repulsion $U < \Delta$, when the sites with lower diagonal energy are doubly occupied, but is a type of Mott insulator (MI) for $U > \Delta$, when all sites are singly occupied. However, for finite, small t , perturbational approaches become invalid at $U = \Delta$ and nontrivial charge fluctuations persist even in the strongly coupled limit. Effective models around this limit have been proposed and analyzed¹⁸ but not yet studied numerically. Nevertheless, following the initial proposal of Fabrizio, Gogolin, and Nersisyan,¹⁰ subsequent numerical studies,^{12,13,16,19} and the obtaining of exact results for a closely related model,^{17,18} it has become clear that the IHM chain has two transitions as U is increased. The first is a charge transition at $U = U_c$, thought to be of the Ising type,^{10,11,19} from the BI to a bond-ordered, spontaneously dimerized, ferroelectric insulator (FI). The second, when U is further increased, involves a vanishing of the spin gap at $U_s > U_c$ at a Kosterlitz-Thouless transition between the FI and the MI.^{10,11} The phase diagram has been constructed in full detail by following the crossing of appropriate excited energy levels, which for this model turns out to be

equivalent to the method of jumps in Berry phases (topological transitions).¹² For finite chains it has been shown that the topological transition at U_c may be detectable in measurements of transport through annular molecules or nanodevices.²⁰

A particularly interesting feature of the model is the ferroelectric nature of the intermediate FI phase.^{17,18,21} This phase results from an electronically induced Peierls instability, which generates a ferroelectric state with no ionic displacement. Interestingly, the elementary excitations of the FI phase have a fractional charge, which is proportional to the polarization.¹⁸ Experimentally, a bond-ordered ferroelectric state has been observed in the pressure-temperature phase diagram of the prototypical compound tetrathiafulvalene-*p*-chloranil.^{3,4} As noted by Ishihara, Egami, and Tachiki,⁵ the microscopic origin of the displacive-type ferroelectric transition in covalent perovskite oxides such as $BaTiO_3$ remains unclear.

The motivation for the present study is to investigate the changes in this type of phase diagram with the periodicity of the lattice, while retaining one electronegative ion and two electrons per unit cell, in such a way that for $U=0$ the system is clearly a BI. However, away from half filling, i.e., for $N > 2$, the conventional Umklapp scattering term, responsible for dynamical generation of a charge gap in the half-filled Hubbard chain, is absent, and therefore one might expect metallic behavior or at minimum some qualitatively different physical properties at larger values of U when $N \neq 2$. The model with $N=3$ may also be relevant for the properties of doped, halogen-bridged binuclear metal chains (referred to as *MMX* chains) such as $R_4[Pt_2(P_2O_5H_2)_4X \cdot nH_2O]$.²² These compounds are related in turn to the quasi-one-dimensional *MX* complexes, which have been of interest for several decades in the broader context of the physics of electronic chain systems.

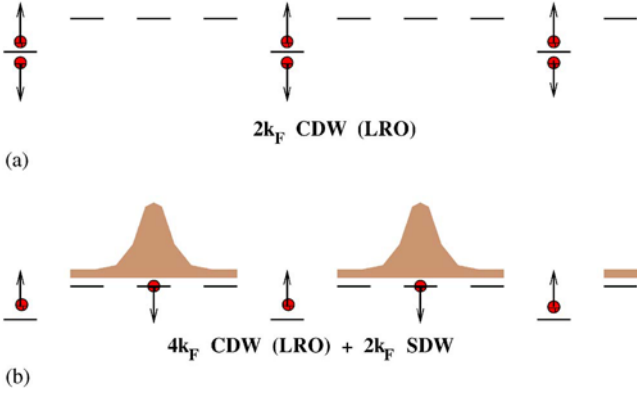


FIG. 1. (Color online) Charge and spin distribution in the strong-coupling limit, illustrated for an AB_3 chain.

The paper is organized as follows. In Sec. II we study the limit $t \rightarrow 0$ to derive some results for the charge and spin gaps, and for the effective spin Hamiltonian. In Sec. III the opposite limit, of weak interactions, is treated by bosonization, and qualitative results are presented for the expected phases and correlation functions. Section IV contains a description of the numerical tools which are used in Sec. V to deduce the quantum phase diagram and to discuss the metallic or insulating character of the system. Section VI contains a summary and discussion.

II. STRONG-COUPLING LIMIT

We begin by expressing the Hamiltonian for the AB_{N-1} chain in a form to be used consistently throughout the following sections:

$$H = -t \sum_{i\sigma} (c_{i+1\sigma}^\dagger c_{i\sigma} + \text{H.c.}) + U \sum_i n_{i\uparrow} n_{i\downarrow} + \sum_i \Delta_i n_i. \quad (1)$$

Here $c_{i\sigma}^\dagger$ creates an electron at site i with spin σ , $n_{i\sigma} = c_{i\sigma}^\dagger c_{i\sigma}$, and $n_i = n_{i\uparrow} + n_{i\downarrow}$. The nearest-neighbor hopping amplitude is denoted by t , U is the on-site Hubbard interaction and $\Delta_i = -\Delta$ if i is a multiple of N and zero otherwise. Thus $\Delta > 0$ is the difference in on-site energies between “metallic” (B or M) and “halogen” (A or X) sites on an AB_{N-1} ($M_{N-1}X$) chain.

A significant part of the physics of the AB_{N-1} chain can be understood by considering the limit of small t . However, as in the case of the conventional IHM ($N=2$), this limit presents particular complications for $U=\Delta$. Although it is possible at this special point to make a canonical transformation retaining three states per site,¹⁸ the resulting Hamiltonian is not trivial and no definitive conclusions may be drawn from it without further numerical analysis. This is beyond the scope of the current investigation, and in the remainder of this section we assume that $|U-\Delta| \gg t$.

For $U < \Delta$, in a treatment discarding terms of order $[t/(\Delta-U)]^2$ the A sites are doubly occupied and the B sites are empty. Thus the charges are ordered in a charge-density wave (CDW) as represented in Fig. 1(a). The physics of this state can be described in terms of a one-particle picture in which the lower band is filled and the others are empty,

yielding a BI. Again neglecting corrections of order t^2 , the charge and spin gap are both equal to $\Delta-U$. We note that in contrast to the case $N=2$, for $N > 2$ the charge distribution is altered radically if Δ is negative, because if $t \ll U$ the double occupancy at any site is no longer of order 1, but of order $(t/U)^2$, but here we will not consider this situation further.

Another simple limit is $\Delta=0$, where from the physics of the Hubbard model it is known that for any value of t the system is a MI for $N=2$ but a Luttinger liquid for any $N > 2$.²³⁻²⁵

A further known result concerns the case $N=2$ and $U-\Delta \gg t$, where the system adopts a form of modified MI state, which we will call here the “correlated insulator” (CI), with almost exactly one particle per site and a charge gap of approximately $U-\Delta$. This state has gapless spin excitations and long-ranged CDW order.^{14,15} In spite of the fact that sites A and B are not equivalent, the system can be described by an effective Heisenberg model which is invariant under a one-site translation interchanging sites A and B.^{2,15} However, the expectation values calculated with this effective Hamiltonian are not invariant under the same one-site translation due to the accompanying mapping of the operators.¹⁵ The charge difference between A and B sites (the amplitude of the CDW) is at lowest order $22.2t^2\Delta U/(U^2-\Delta^2)^2$ and the decay of the charge-charge correlation function with distance d has the form $d^{-3} \ln^{-3/2}d$ for large d , with a prefactor proportional to $t^4\Delta^2$.^{15,16}

In order to extract analogous results for the case $N > 2$, we begin by considering the limit $U \rightarrow +\infty$, where the Hamiltonian for any N can be mapped to a noninteracting spinless system with an effective magnetic flux.^{26,27} For $N > 2$ and any positive Δ , the system is an insulator with a charge distribution of the form depicted in Fig. 1(b). We will refer to this state as a CI to distinguish it from the charge distribution of the unperturbed MI. The primary differences from the case of the CI for $N=2$ are that a finite value of Δ is required to drive the system into an insulating state, and that the gap in this state is very small. For $U \rightarrow +\infty$ and $N > 2$, this gap is given by

$$E_c = 2t\{\cos[\pi/N] - \cos[2\pi/N]\} \quad \text{if } \Delta \gg t,$$

$$E_c = 2\Delta/N \quad \text{if } \Delta \ll t. \quad (2)$$

For $N > 2$ and $U-\Delta \gg t$ but with finite U , the spin degrees of freedom are important. A canonical transformation which eliminates doubly occupied sites maps the model into a generalized t - J model

$$\begin{aligned} H = & -t \sum_{i\sigma} P(c_{i+1\sigma}^\dagger c_{i\sigma} + \text{H.c.})P + \sum_i \Delta_i n_i \\ & + \sum_{i\delta=\pm 1} t_i^{ch} P \left[c_{i+\delta\sigma}^\dagger c_{i-\delta\sigma} \left(2\mathbf{s}_i \cdot \mathbf{s}_{i-\delta} - \frac{1}{2}n_i \right) \right] P \\ & + \sum_i J_i \left(\mathbf{s}_i \cdot \mathbf{s}_{i+1} - \frac{1}{4}n_i n_{i+1} \right), \end{aligned} \quad (3)$$

where $P = \prod_i (1 - n_{i\uparrow} n_{i\downarrow})$ is the projector on the subspace of no double occupancy. The exchange parameter is given by

$$J_i = \frac{4t^2 U}{U^2 - \Delta^2} \quad \text{for } i = lN \text{ or } i = lN - 1,$$

$$J_i = \frac{4t^2}{U} \quad \text{otherwise,} \quad (4)$$

where l is an integer, and the correlated hopping term by

$$t_i^{ch} = \frac{t^2}{U - \Delta} \quad \text{for } i = lN, \quad (l \text{ integer}),$$

$$t_i^{ch} = \frac{1}{2} \left(\frac{t^2}{U} + \frac{t^2}{U + \Delta} \right) \quad \text{for } i = lN + 1 \text{ or } i = lN - 1,$$

$$t_i^{ch} = \frac{t^2}{U} \quad \text{otherwise.} \quad (5)$$

As in the Hubbard model,²⁸ for the effective model of Eq. (3) the charge degrees of freedom are independent of the spin of the particles in the limit $U \rightarrow +\infty$, and can be described by a single Slater determinant corresponding to spinless fermions. The terms proportional to J_i and t_i^{ch} can be treated as a perturbation, and the resulting effective Hamiltonian H_s for the spin degrees of freedom takes the form of a Heisenberg model for a “squeezed” chain, by which is meant one in which the empty sites are eliminated and the number of sites is equal to the number of electrons. The effective model H_s is similar to generalized t - J models which have been studied previously,^{29,30} with one important exception: because J_i and t_i^{ch} depend on the site, and the electrons which carry the spin are mobile (filling less than $1/2$ for $N > 2$), the effective exchange term depends on the charge configuration. However, because the effective hopping t is much larger than J_i and t_i^{ch} for $U - \Delta \gg t$ (i.e., the charge velocity is much larger than the spin velocity), it is reasonable to assume that all spin degrees of freedom experience an average effective exchange interaction.

Thus one may write

$$H_s = \sum_i J_{\text{eff}} \left(\mathbf{s}_i \cdot \mathbf{s}_{i+1} - \frac{1}{4} \right), \quad (6)$$

where

$$J_{\text{eff}} = \frac{1}{N} \sum_{i=0}^{N-1} [J_i \langle n_i n_{i+1} \rangle' + 2t_i^{ch} \langle c_{i-1}^\dagger c_{i+1} n_i \rangle' + 2t_{i+1}^{ch} \langle c_{i+2}^\dagger c_i n_{i+1} \rangle'] \quad (7)$$

and the expectation values $\langle O \rangle'$ of the operator O are evaluated in the spinless model. It is well known that H_s has a gapless spectrum with algebraic decay of the spin-spin correlation function and only short-ranged antiferromagnetic order, as represented in Fig. 1(b).

In the effective Hamiltonian of Eq. (6) we have included only terms up to order t^2 which break the spin degeneracy of the $U \rightarrow +\infty$ limit. However, a next-nearest-neighbor exchange interaction J' appears at fourth order in t in the conventional IHM ($N=2$),² and as U is decreased the quantity J' increases faster than J_{eff} does. It is known that a spin gap

opens for $J'/J > 0.2411\dots$ in this spin model,³¹ and thus a transition to a spin-gapped phase is expected as U is lowered.¹⁴ One then expects that for $N > 2$ the presence of terms of higher order in t which are not included in Eq. (6) also drive the same sort of spin transition as U is lowered away from the strong-coupling limit.

To summarize the results of this section, from a strong-coupling analysis of the AB_{N-1} chain one may conclude that, for fixed, finite Δ and small U , in the limit $t \rightarrow 0$ the system has a BI phase. As U increases, the spin gap decreases within the BI regime and vanishes near $U \sim \Delta$, as in the conventional IHM. For higher values of U the system adopts a CI phase which is similar to the MI in that charge degrees of freedom are high-lying and an effective spin model (albeit residing on a CDW background) describes the low-energy physics. However, from these considerations it is not possible to deduce the presence or absence of an intermediate FI phase.

III. WEAK-COUPLING LIMIT

In this section we analyze the model of Eq. (1) using bosonization, a technique which is applicable in the limit $(U, \Delta) \ll t$. A conventional weak-coupling analysis implies a small interaction U , but in this case one may not expand around the noninteracting case ($U=0$) with $\Delta > 0$ because in this regime the system is a BI and has no Fermi points. Instead, for $U=\Delta=0$ the AB_{N-1} model reduces to a noninteracting chain with band filling $1/N$ (two particles in N sites), for which the Fermi wave vector and Fermi velocity are given by

$$k_F = \frac{\pi}{Na_0} \quad \text{and} \quad v_F = 2ta_0 \sin(a_0 k_F), \quad (8)$$

respectively, where a_0 is the lattice spacing.

As in the conventional IHM ($N=2$), the bosonized expression for the Δ term [Eq. (24)] is strongly relevant, and renders the usual renormalization-group treatment of the model³² invalid. For $N=2$ some approximate and phenomenological treatments have predicted the existence of the FI phase and its fractionally charged excitations.^{10,11,18} In particular, by starting from the CI phase and integrating approximately over the charge degrees of freedom, Fabrizio, Gogolin, and Nersesyan predicted that the spin transition takes place at a larger value of the on-site repulsion (U_s) than the charge transition (U_c) does.¹⁰ Taking the effective potential obtained from bosonization as a phenomenological Ginzburg–Landau free energy, these authors found that the excitations in the FI phase have a fractional charge which varies between 1 at the boundary with the BI phase and 0 at the boundary with the CI phase. Thus the elementary excitation interpolates between an electron in the BI phase and a spinon in the CI phase, and its fractional charge is proportional to the electric polarization in the FI phase.¹⁸ These excitations may be visualized as the topological excitations of an effective spin-1 chain for $t \ll U, \Delta$.^{17,18}

In the same spirit as the analysis of Fabrizio and co-workers, we identify the most important operators for $N > 2$

chains on the basis of their critical dimensions and their expected effect on the physics. From these we infer the qualitative features of the phase diagram, which will be compared with numerical results in Sec. V.

We linearize the spectrum and pass to the continuum limit by the substitution

$$c_{j\sigma} \rightarrow \sqrt{a_0} [e^{ik_F x} \Psi_{+, \sigma}(x) + e^{-ik_F x} \Psi_{-, \sigma}(x)], \quad (9)$$

where the original lattice operators are decomposed into right- and left-moving components $\Psi_{+, \sigma}^\dagger(x)$ and $\Psi_{-, \sigma}^\dagger(x)$, and $x = ja_0$. Bosonization of these fields by a standard method for electrons with spin^{33,34} yields

$$\Psi_{\pm, \sigma}^\dagger(x) \simeq \frac{\kappa_{\pm, \sigma}^\dagger}{\sqrt{2\pi a_0}} \exp(\mp i\phi_{\pm\sigma} + \theta_{\pm\sigma}), \quad (10)$$

where $\phi_{+\sigma}$ ($\phi_{-\sigma}$) are right- (left)-moving Bose fields and $\theta_{r\sigma}$ is the field dual to $\phi_{r\sigma}$. The Klein factors $\kappa_{r\sigma}^\dagger$ have the physical meaning of ladder operators which increase by one the number of fermions in branch r with spin σ , and also serve to ensure that the anticommutation relations for electron fields of different spin are maintained. They are Hermitian and satisfy a Clifford algebra³⁵

$$\begin{aligned} \{\kappa_{+\sigma}, \kappa_{+\sigma'}\} &= \{\kappa_{-\sigma}, \kappa_{-\sigma'}\} = 2\delta_{\sigma\sigma'} \\ \{\kappa_{+\sigma}, \kappa_{-\sigma'}\} &= 0. \end{aligned} \quad (11)$$

We define

$$\phi_\sigma = \phi_{-\sigma} + \phi_{+\sigma}, \quad \theta_\sigma = \phi_{-\sigma} - \phi_{+\sigma}$$

and introduce the linear combinations

$$\phi_c = \frac{1}{\sqrt{2}}(\phi_\uparrow + \phi_\downarrow), \quad \theta_c = \frac{1}{\sqrt{2}}(\theta_\uparrow - \theta_\downarrow) \quad (12)$$

$$\phi_s = \frac{1}{\sqrt{2}}(\phi_\uparrow - \phi_\downarrow), \quad \theta_s = \frac{1}{\sqrt{2}}(\theta_\uparrow + \theta_\downarrow) \quad (13)$$

to describe, respectively, the charge (ϕ_c) and spin (ϕ_s) degrees of freedom and their conjugate momenta.

With the exception of the term in \mathcal{A}_{4k_F} below, the above equations combined with appropriate operator product expansions give the bosonized expressions for the charge density

$$\begin{aligned} \rho_c(x) \equiv :n_{i\uparrow} + n_{i\downarrow}: &\rightarrow \frac{1}{\sqrt{2\pi}}(\partial_x \phi_c) \\ &+ \mathcal{A}_{2k_F} \cos(2k_F x + \sqrt{2}\phi_c) \cos \sqrt{2}\phi_s \\ &- \mathcal{A}_{4k_F} \cos(4k_F x + \sqrt{8}\phi_c) \end{aligned} \quad (14)$$

and for the spin density

$$\begin{aligned} \rho_s(x) \equiv \frac{1}{2}(n_{i\uparrow} - n_{i\downarrow}): &\rightarrow \frac{1}{\sqrt{2\pi}}(\partial_x \phi_s) \\ &+ \mathcal{B}_{2k_F} \cos(2k_F x + \sqrt{2}\phi_c) \sin \sqrt{2}\phi_s. \end{aligned} \quad (15)$$

The term in \mathcal{A}_{4k_F} , which is crucial in our analysis, is not

present in a standard bosonization procedure but is generated in any model with density-density interaction terms. This may be seen by considering the lowest-order correction in the dressed charge operator, which includes terms of the form $e^{-4ik_F} \Psi_{+, \sigma}^\dagger \Psi_{+, \sigma}^\dagger \Psi_{-, \sigma} \Psi_{-, \sigma}$, where each electron operator $c_{j\sigma}^\dagger$ contributing to the four-fermion product introduces a factor of e^{-ik_F} [see Eq. (9)]. The presence of this term has been established definitively in the Hubbard model (any AB_{N-1} chain with $\Delta=0$).³⁶

The coefficients \mathcal{A}_{2k_F} , \mathcal{A}_{4k_F} , and \mathcal{B}_{2k_F} are nonuniversal parameters which depend on U and fulfil the conditions

$$\begin{aligned} \lim_{U \rightarrow 0} \mathcal{A}_{2k_F}(U) &= \mathcal{A}_1^0 = \frac{1}{2\pi}, \\ \lim_{U \rightarrow 0} \mathcal{B}_{2k_F}(U) &= \frac{1}{2} \mathcal{A}_1^0, \\ \lim_{U \rightarrow 0} \mathcal{A}_{4k_F}(U) &= 0, \\ \lim_{U \rightarrow +\infty} \mathcal{A}_{4k_F}(U) &= \mathcal{A}_1^0. \end{aligned} \quad (16)$$

The coefficient \mathcal{A}_{4k_F} has been calculated numerically for the particular case of the 0.55-filled Hubbard chain.³⁶ It has a monotonic behavior, linear in U for $U \rightarrow 0$ and with a downward curvature. For $U=10t$ it is of order 0.12, already close to its saturation value $\mathcal{A}_1^0 \simeq 0.159$ for $U \rightarrow +\infty$. For the filling $1/N$ under consideration [two particles per unit cell, Eq. (8)], a $2k_F$ modulation corresponds to the periodicity of the AB_{N-1} lattice, while $4k_F$ corresponds to a modulation of half this period in real space (Fig. 1).

To derive the bosonized expression of the on-site energy term in the continuum limit, we note that it can be written in the form

$$\sum_j \Delta_j n_j = -\frac{\Delta}{N} \sum_j \sum_{l=0}^{N-1} \exp(2ik_F a_0 l j) n_j. \quad (17)$$

By transforming the sum over j into an integral over $x = ja_0$, using Eq. (14), and neglecting rapidly oscillating factors [which here means retaining only those terms in $\exp(ik_F a_0 n)$ with n a multiple of $2N$], we obtain

$$\begin{aligned} \sum_j \Delta_j n_j &\rightarrow -\frac{\Delta}{N} \mathcal{A}_{2k_F} \int dx \cos(\sqrt{2}\phi_c) \cos(\sqrt{2}\phi_s) \\ &+ \frac{\Delta}{N} \mathcal{A}_{4k_F} \int dx \cos(\sqrt{8}\phi_c). \end{aligned} \quad (18)$$

For the interaction term, with $N > 2$ one obtains the usual form

$$U \sum_i n_{i\uparrow} n_{i\downarrow} \rightarrow \int dx \left\{ \frac{U}{2\pi^2} [(\partial_x \phi_c)^2 - (\partial_x \phi_s)^2] + \frac{U}{(2\pi a_0)^2} \cos(\sqrt{8}\phi_s) \right\}. \quad (19)$$

Only for $N=2$ does one have in addition the contribution from Umklapp scattering processes

$$\mathcal{H}_{\text{Um}} = \frac{U}{(2\pi a_0)^2} \int dx \cos(\sqrt{8}\phi_c), \quad (20)$$

which has the same form as the last term in Eq. (18). We note that, even at weak coupling where the bosonization results are applicable, $U \gg \Delta \mathcal{A}_{4k_F}$ and \mathcal{H}_{Um} is the dominant term in the $N=2$ case.¹⁰

On including the noninteracting part, the final Hamiltonian density for the bosonized model can be expressed as

$$\mathcal{H}_{\text{eff}} = \mathcal{H}_c + \mathcal{H}_s + \mathcal{H}_{cs}, \quad (21)$$

$$\mathcal{H}_c = \frac{\pi v_c K_c}{2} \Pi_c^2(x) + \frac{v_c}{2\pi K_c} (\partial_x \phi_c)^2 + \frac{M_c}{(2\pi a_0)^2} \cos(\sqrt{8}\phi_c(x)), \quad (22)$$

$$\mathcal{H}_s = \frac{\pi v_s}{2} \Pi_s^2(x) + \frac{v_s}{2\pi} (\partial_x \phi_s)^2 + \frac{M_s}{(2\pi a_0)^2} \cos(\sqrt{8}\phi_s(x)), \quad (23)$$

$$\mathcal{H}_{cs} = -\frac{m_{cs}}{\pi a_0} \cos(\sqrt{2}\phi_c) \cos(\sqrt{2}\phi_s). \quad (24)$$

Here Π_v is the moment conjugate to ϕ_v , v_c and v_s are the charge and spin velocities, and K_c is the charge-correlation exponent. For small interactions, the values of the different parameters are

$$\begin{aligned} M_c &\simeq U \quad \text{if } N=2, \\ M_c &\simeq \Delta \cdot \mathcal{A}_{4k_F}(U) \quad \text{if } N>2, \\ K_c &\simeq 1 - U a_0 / \pi v_F, \quad v_c, v_s \simeq v_F \\ M_s &\simeq U, \quad m_{cs} \simeq \Delta. \end{aligned} \quad (25)$$

This Hamiltonian density coincides formally with the field theory studied previously^{10,11} for the case $N=2$ corresponding to the IHM, with the sole difference arising in the amplitude of the effective Umklapp scattering term M_c .

To discuss properties of the different phases which appear in the AB_{N-1} model, in addition to the on-site charge and spin density operators defined in Eqs. (14) and (15), we will use the bosonized expressions for the on-bond charge and spin density operators,^{37,38}

$$\begin{aligned} B_i &= \sum_{\sigma} (c_{i,\sigma}^{\dagger} c_{i+1,\sigma} + c_{i+1,\sigma}^{\dagger} c_{i,\sigma}) \rightarrow \frac{1}{2\pi} [\Pi_c^2(x) + (\partial_x \phi_c)^2] \\ &+ \cos((2i+1)\pi/N + \sqrt{2}\phi_c) \cos \sqrt{2}\phi_s, \end{aligned} \quad (26)$$

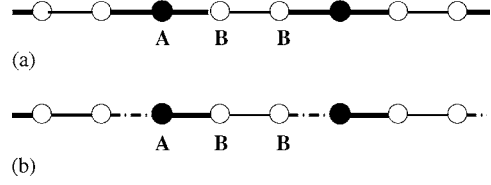


FIG. 2. Bond-density distribution (a) in the BI phase and (b) in the FI phase of an AB_2 chain. Thick lines correspond to high on-bond density, thin lines to less occupied bonds, and dashed lines to bonds with lowest occupation.

$$\begin{aligned} W_i &= \sum_{\sigma} \sigma (c_{i,\sigma}^{\dagger} c_{i+1,\sigma} + c_{i+1,\sigma}^{\dagger} c_{i,\sigma}) \rightarrow \frac{1}{2\pi} [\Pi_s^2(x) + (\partial_x \phi_s)^2] \\ &+ \cos((2i+1)\pi/N + \sqrt{2}\phi_c) \sin \sqrt{2}\phi_s. \end{aligned} \quad (27)$$

To characterize the FI phase we introduce the order parameter

$$\mathcal{O}_{\text{FI}} = \sum_j \cos(2k_F a_0 j) (B_j - B_{j-1}),$$

which represents the $2k_F$ Fourier component of the difference between consecutive bond-density operators, and whose bosonized expression takes the form

$$\mathcal{O}_{\text{FI}} \simeq \sin(\pi/N) \sin(\sqrt{2}\phi_c) \cos(\sqrt{2}\phi_s). \quad (28)$$

We note that the operator \mathcal{O}_{FI} is antisymmetric with respect to inversion at the A sites ($j \rightarrow -j$).

Classically, it is clear that minimization of the ionic term in Eq. (24) requires either $\phi_c = \phi_s = 0$ or $\sqrt{2}\phi_c = \sqrt{2}\phi_s = \pi \pmod{2\pi}$. These values of ϕ_c and ϕ_s characterize the BI phase, as they ensure that bond-order parameter \mathcal{O}_{FI} and the site and bond spin densities [Eqs. (15) and (27)] are suppressed, while there remains a long-ranged CDW order at $2k_F$ [Eq. (14)] with increased charge on the A atoms (for which x is multiple of $N a_0$). The amplitude of the $4k_F$ CDW is much smaller because it is proportional to \mathcal{A}_{4k_F} . We stress that due to the symmetry of the Hamiltonian a $2k_F$ CDW is present in all phases of the model. In contrast to the $N=2$ case there is also a modulation of the bond order, or bond-order wave, in the BI phase with $B_i \propto \cos[(2i+1)\pi/N]$ (26) as a consequence of the N -site unit cell. This distribution of bond intensities is represented in Fig. 2(a), and is symmetric under reflection at the A sites ($\mathcal{O}_{\text{FI}}=0$).

While $\sqrt{8}\phi_c = 0 \pmod{2\pi}$ in the BI phase, minimizing the potential of \mathcal{H}_c [Eq. (22)] requires $\sqrt{8}\phi_c = \pi \pmod{2\pi}$. Thus for fixed Δ there is a charge transition with increasing U for $N=2$.^{10,11} For $N>2$, M_c is determined not only by the on-site repulsion U but also by the ionicity parameter Δ . At small U , $M_c \simeq \Delta U/t$, but for large U one expects $M_c \simeq \Delta$ as a result of the saturation of $\mathcal{A}_{4k_F}(U)$ in the Hubbard model (above). In consequence it is not possible to assure, as in the case $N=2$, that this effect will overcome the ionicity for sufficiently large on-site repulsion, leading to a transition in the charge sector. However, from the results of the previous section, in the strong-coupling limit ($t \rightarrow 0$) there is a charge transition for $U=U_c$ with $U_c \sim \Delta$. There is also a spin transition at $U=U_s$ because the BI phase has a spin gap which vanishes

when $U - \Delta \gg t$. Thus it appears that the same generic phase diagram indeed emerges for all values of N .

For $N=2$, the authors of Ref. 10 argued that $U_s > U_c$ by describing the charge degrees of freedom in the CI phase in terms of a free boson of mass (charge gap) E_c . On integrating over the charge degrees of freedom, the resulting effective Hamiltonian takes the form of Eq. (23) but with an effective renormalized mass

$$M'_s - M_s \simeq -8\pi t(\Delta/E_c)^2, \quad (29)$$

whence U_s is determined by the condition $M'_s = 0$. For $U_c < U < U_s$ the system retains a spin gap as in the BI phase, with the values $\varphi_s = 0$ or $\varphi_s = \pi/\sqrt{2}$ frozen, but the nature of the charge sector has changed. The spin correlations still decay exponentially due to the presence of the spin gap.

An analysis of the intermediate regime may be performed for higher values of N by analogy with that applied to the model with $N=2$. This type of treatment^{10,18} shows that the intermediate phase is characterized in the bosonized description by values of $\sqrt{8}\phi_c$ intermediate between 0 and π , and thus possesses fractional-charge excitations, broken inversion symmetry, and the nonzero polarizability of a ferroelectric phase. Because $\phi_c \neq 0$, one observes from Eq. (28) that the order parameter is finite, $\mathcal{O}_{\text{FI}} \neq 0$, meaning that the charge distribution in the intermediate phase is characterized by broken inversion symmetry at the A sites. The long-ranged order of the BI phase, namely the $2k_F$ modulation of the site charge density and the N -site-periodic modulation of the bond density, is retained. The distribution of bond charge density resulting from Eq. (26) for one of the two possible inequivalent choices of ϕ_v , minimizing the energy is represented in Fig. 2(b), which makes clear the spontaneous breaking of parity in the FI phase.

Qualitatively, the properties of the FI phase may be understood in this framework by taking the interaction part of the Hamiltonian density as a phenomenological Ginzburg–Landau energy functional with effective interactions.¹⁰ In the notation chosen here,³⁵ this energy functional takes the form¹⁸

$$F = M_c \alpha_c^2 + M_s \alpha_s^2 + m_{cs} \alpha_c \alpha_s, \quad (30)$$

with $\alpha_v = \cos(\sqrt{2}\phi_v)$,

with $M_s < 0$, $M_c > 2m_{cs}$, and all parameters duly renormalized. The minima of F occur when $\alpha_c = m_{cs}/(2M_c)$, $\alpha_s = -1$, or $\alpha_c = -m_{cs}/(2M_c)$, $\alpha_s = 1$. A soliton between two segments of the system characterized by these pairs of values corresponds to an elementary excitation of spin 1/2 and charge $C = 1 - 2 \arccos[m_{cs}/(2M_c)]/\pi$ (i.e., proportional to the difference between the two values of ϕ_c). The polarization of the homogeneous system turns out to be $\pm eC/2$.¹⁸

Finally, for $U > U_s$, the spin gap is absent and the system is in the CI phase. With increasing on-site repulsion the amplitude of the $2k_F$ modulations of the on-site charge density, \mathcal{A}_{2k_F} , decreases and the $4k_F$ component becomes dominant. Because of the spatial modulation of Δ there is long-ranged CDW order in the ground state^{14,15} as when $N=2$. However, on top of this order the system also possesses the antiferro-

magnetic spin ordering represented in Fig. 1(b). As a consequence of the gapless character of the spin excitations, all correlation functions decay with a power-law form, including fluctuations of the charge density because of the strong charge-spin coupling [Eq. (24)]. These correlation functions have been considered by one of us for the case $N=2$.¹⁵

We conclude this section by extracting from the form of the bosonized effective Hamiltonian (21) the following differences between the well-characterized AB system and the AB_{N-1} chain with $N > 2$:

(1) Because the amplitude of M_c is very much smaller than for the AB chain, the BI gap decreases more slowly with increasing U and the BI phase should extend to larger values of U .

(2) The charge gap E_c in the CI phase ($U > U_s$) is determined not only by U but also by the ionicity parameter Δ . In particular, because the amplitude $\mathcal{A}_{4k_F}(U)$ of the $4k_F$ modulations saturates for large U , one expects that E_c is determined solely by Δ and t for $U \rightarrow +\infty$, in agreement with the results of the previous section.

(3) The smaller value of E_c implies a larger renormalization of the effective spin mass M'_s [Eq. (29)], and thus the FI phase is expected over a wider parameter range.

IV. NUMERICAL METHODS

We have performed numerical calculations of a number of quantities characterizing the physical properties of AB_{N-1} chains for comparison with the analytical considerations of Secs. II and III, and to interpolate between the limits these represent. Here we describe the numerical techniques applied to the Hamiltonian of Eq. (1).

We have determined numerically the phase diagram for systems of L sites by considering the crossing of appropriate excited energy levels which correspond to jumps in the charge (γ_c) and spin (γ_s) Berry phases, and by computing the charge (z_c^i) and spin (z_s^i) localization parameters defined below. We have in addition calculated the Drude weight D_c in some cases as a supplementary probe of metallic behavior.

The parameter γ_c is the Berry phase captured by the ground state for a ring threaded by a flux which is varied adiabatically from zero to two flux quanta.^{39–41} The spin Berry phase γ_s is the corresponding quantity for a situation in which oppositely directed fluxes are experienced by spin-up and spin-down particles.^{42–44} Specifically, under an applied flux (which we have scaled to be dimensionless) $\Phi_\sigma hc/(2\pi e)$ for spin σ , the Hamiltonian H [Eq. (1)] is transformed into a Hamiltonian \tilde{H} which differs from H in that the hopping term has the form $-t \sum_{i\sigma} (\tilde{c}_{i+1\sigma}^\dagger \tilde{c}_{i\sigma} e^{i\Phi_\sigma/L} + \text{H.c.})$. We denote by $|g(\Phi_\uparrow, \Phi_\downarrow)\rangle$ the ground state of $\tilde{H}(\Phi_\uparrow, \Phi_\downarrow)$. The charge (spin) Berry phase γ_c (γ_s) is the overall phase captured by the state $|g(\Phi_\uparrow, \Phi_\downarrow)\rangle$ on following adiabatically the cycle $0 \leq \Phi \leq 2\pi$ with $\Phi_\uparrow = \Phi_\downarrow = \Phi$ ($\Phi_\uparrow = -\Phi_\downarrow = \Phi$). Discretizing the interval $0 \leq \Phi \leq 2\pi$ into $N+1$ points $\Phi_r = 2\pi r/N$ ($r=0, N$), the Berry phases are calculated from the numerically gauge-invariant expression⁴¹

$$\gamma_{c(s)} = \lim_{N \rightarrow \infty} \text{Im} \left\{ \ln \left[\prod_{r=0}^{N-2} \langle g(\Phi_r, \pm \Phi_r) | g(\Phi_{r+1}, \pm \Phi_{r+1}) \rangle \right. \right. \\ \left. \left. \times \langle g(\Phi_{N-1}, \pm \Phi_{N-1}) | g(2\pi, \pm 2\pi) \rangle \right] \right\}. \quad (31)$$

The state $|g(2\pi, 2\pi)\rangle$ ($|g(2\pi, -2\pi)\rangle$) is obtained from $|g(0, 0)\rangle$ by applying the displacement operator U_L^c (U_L^s),

$$|g(2\pi, \pm 2\pi)\rangle = U_L^{c(s)} |g(0, 0)\rangle, \quad (32)$$

with

$$U_L^c = \exp \left[i \frac{2\pi}{L} X \right], \quad X = \sum_j ja_0(n_{j\uparrow} + n_{j\downarrow}), \quad (33)$$

$$U_L^s = \exp \left[i \frac{2\pi}{L} D \right], \quad D = \sum_j ja_0(n_{j\uparrow} - n_{j\downarrow}). \quad (34)$$

Note that Eq. (32) is simply a gauge transformation which transforms the ground state of H into that of $\tilde{H}(2\pi, \pm 2\pi)$. The operator U_L^c , the exponential of the total-position operator, constitutes a translation in momentum space which displaces all single-particle wave vectors by $2\pi/L$.⁴⁵ Similarly, U_L^s displaces the wave vectors of up and down particles in opposite directions.

An important property of the charge Berry phase is that if the system is modified by some perturbation, the change in polarization $P_{\uparrow} + P_{\downarrow}$ is proportional to the corresponding change in γ_c .⁴⁰ Here P_{σ} is the contribution of electrons with spin σ to the polarization of the system. Similarly, changes in γ_s are related to changes in the difference $P_{\uparrow} - P_{\downarrow}$ between the electric polarizations for up and down spins⁴²

$$\Delta P_{\uparrow} \pm \Delta P_{\downarrow} = e \Delta \gamma_{c(s)} / 2\pi \pmod{e}. \quad (35)$$

The AB_{N-1} chain has site inversion symmetry at the A sites for all N , and also at the B sites for $N=2$. A crucial property for the purposes of the present analysis is that, in systems with site inversion symmetry, γ_c and γ_s can only take the values 0 or $\pi \pmod{2\pi}$ [the argument of the logarithm in Eq. (31) becomes its own complex conjugate under inversion]. Thus the Berry-phase vector $\gamma = (\gamma_c, \gamma_s)$ cannot vary continuously, and a jump in γ corresponds to a transition in at least one of the topological quantum numbers γ_c/π and γ_s/π . These topological transitions usually correspond to phase transitions in the thermodynamic limit. As an example, in the strong-coupling limit the CI phase of the IHM has one charge at every site (1111...), while the BI is characterized by a charge distribution of alternating electron pairs (2020...). In order to transform from one to the other it is necessary to displace half of the charges by one lattice parameter, which corresponds to a change $\pm e/2$ in the polarization of the system, and according to Eq. (35) the transition is accompanied by a jump of π in γ_c . Similarly, it can be shown that the opening of a spin gap in a Luttinger-liquid phase of a spin-rotationally invariant model is accompanied by a topological transition in γ_s .⁴² Extrapolating the parameters for which these jumps occur in systems with $L \leq 16$ to the thermodynamic limit has led to a very accurate determi-

nation of the quantum phase diagram of the Hubbard model with correlated hopping.^{43,44} Other successful applications of the method include the extended Hubbard chain with charge-dipole interactions⁴¹ and the conventional IHM¹² ($N=2$ of the present case).

In the limit in which all charges are localized (generally the strong-coupling limit), the Berry phases are easy to calculate analytically. For $t=0$ one may choose a gauge in which all scalar products in Eq. (31) are equal to 1, except possibly the last. The Berry phases are then defined by the argument of the exponential of $U_L^{c(s)}$ in Eq. (32). An illustrative example is the charge distribution of the BI for $t \rightarrow 0$ [Fig. 1(a)] in a system of M unit cells each of length N , such that $L=MN$: it is clear that $D=0$ (34) and thus $\gamma_s=0$, while [see Eq. (33)]

$$X = \sum_{l=0}^{M-1} 2Nl = NM(M-1),$$

whence $U_L^c = \exp[2\pi i(M-1)] = 1$ and $\gamma_c = 0 \pmod{2\pi}$. By contrast, for a system of particles with spin up localized at sites $0, N, 2N, \dots$ and those with spin down localized at positions $N/2, N+N/2, 2N+N/2, \dots$ [Fig. 1(b)], $X = NM(M-1) + NM/2$ and $D = -NM/2$, leading to $U_L^c = U_L^s = -1$ and $\gamma_c = \gamma_s = \pi$; these values characterize the CI.

The jumps in the Berry phases coincide in general with the crossing of pairs of low-lying excited states of a finite system. Thus the critical values U_c and U_s may be determined by the method of crossing excitation levels (MCELs), where this method is construed in a broader sense to be defined below. The relevant level crossing is found where the energy of the ground state $|g(\Phi, \pm \Phi)\rangle$ as a function of the flux Φ reaches its maximum value.¹² This is usually equivalent to the situation obtained by taking boundary conditions (BCs) opposite to the ‘‘closed-shell’’ choice which leads to the minimum energy.¹² Identifying the two crossing levels by their quantum numbers and finding the parameters for which their energies coincide is naturally equivalent to locating the jump in the Berry phase, and the former procedure saves computer time by avoiding the evaluation of Eq. (31). Thus we have followed this method in determining the majority of the data to be shown in Sec. V, although we have also used Eq. (31) for verification of our results.

In its more restricted sense, the MCEL is based on identifying the appropriate levels by conformal field theory with renormalization-group analysis.^{31,46,47} This is a weak-coupling approach which takes advantage of the fact that in conformally invariant systems of finite size the smallest excitation gap corresponds to the dominant correlations at large distances. In previous studies, which included the Hubbard model with correlated hopping,^{43,44,46} the extended Hubbard model,^{12,46} and the conventional IHM,¹² the restricted MCEL and the jumps of Berry phases were found to coincide, giving support to the method from both weak- and strong-coupling analyses.

From the arguments presented in the strong-coupling limit, it is evident that the jump in γ_c characterizes a sharp transition with a reordering of charge. One might expect by continuity that this jump characterizes the charge transition

also at weak coupling. While in previous studies (above) the jump in γ_c does coincide with the crossing of appropriate excitations determined from field-theoretical arguments,^{12,46} for larger N it is not known whether the level crossing which corresponds to the jump in γ_c has support from a weak-coupling approach. In the following, the MCEL refers more broadly to a crossing which corresponds to the jump in a Berry phase, but in the case of γ_c this correspondence is not justified by field-theoretical methods. When considering γ_s in any model with SU(2) symmetry, this crossing always coincides with that corresponding to the Kosterlitz–Thouless transition for the opening of a spin gap according to conformal field theory.⁴²

The specific crossing levels in the MCEL are determined by the quantum numbers specifying their parity, spin, and total momentum, plus the BCs for which the crossing occurs. The spin transition is determined from the crossing of an even singlet and an odd triplet excited state, both with total momentum $K=0$, when working with open-shell BCs. This is the crossing which corresponds to the jump in the spin Berry phase⁴² and has support from field-theoretic arguments.^{31,46} The charge transition is determined from the crossing of an even and an odd singlet, both with $K=\pi/a_0$, again calculated with open-shell BCs. This crossing signals the jump in the charge Berry phase, which as explained above denotes a reordering of charge leading to a jump in the polarization of the system. However, as in other recent calculations in which crossing of levels was used to determine phase transitions in two-dimensional spin systems,^{48,49} a systematic demonstration that this procedure should remain valid in the weak-coupling limit is lacking. For this reason, and because of other shortcomings described below, we reinforce the results obtained from the MCEL by comparison with those obtained from the localization operators.

The localization operators are obtained from the expectation values of the displacement operators

$$z_L^{c(s)} = \langle g | U_L^{c(s)} | g \rangle. \quad (36)$$

$|z_L^c|$ was first proposed by Resta and Sorella as an indicator of localization in extended systems.⁸ By appealing to symmetry properties, Ortiz and one of the authors demonstrated that for translationally invariant interacting systems with a rational number n/l of particles per unit cell the correct definition of the matrix element is $\langle g | (U_L^c)^l | g \rangle$.⁴⁵ This definition was used to characterize metal-insulator and metal-superconducting transitions in one-dimensional lattice models.^{44,45,50} In the thermodynamic limit, $L \rightarrow \infty$, $|z_L^c|$ is equal to 1 for a periodic metallic system and to 0 for the insulating state. This result holds also for noninteracting disordered systems.⁵⁰ For an intuitive understanding we note that in a metallic system with a well-defined Fermi surface, U_L^c displaces the Fermi surface by a wave vector $2\pi/L$, and thus $\langle g | U_L^c | g \rangle = 0$. By contrast, in a noninteracting band insulator $U_L^c | g \rangle$ coincides with $|g\rangle$ and $z_L^c = 1$.

The determination of $z_L^{c(s)}$ in the thermodynamic limit provides a means of calculating the Berry phases^{8,42,44,45,50}

$$\gamma_{c(s)} = \lim_{L \rightarrow \infty} \text{Im} \ln z_L^{c(s)}. \quad (37)$$

For finite L , the right-hand side of Eq. (37) is actually equivalent to Eq. (31) if only a single point is used in the discretization of the flux. Thus it is not surprising that direct calculation of the Berry phase (or the MCEL) leads to a more precise extrapolated result than does Eq. (37).^{44,45} For comparison with these two types of analysis we have performed calculations of $z_L^{c(s)}$, as it emerges that these are important in determining the phase diagram of the AB₃ model at low values of Δ . In addition, the displacement operators have a direct relationship with the bosonic fields introduced in Sec. III: it was shown recently that U_L^c and U_L^s can be constructed as exponentials of the average charge and spin fields¹⁸

$$U_L^v = \exp(i\sqrt{8}\phi_v^a), \quad \phi_v^a = \frac{1}{L} \int dx \phi_v^a(x). \quad (38)$$

In the region of parameters such that the interaction M_c in Eq. (22) is much greater than m_{cs} [Eq. (24)], $\phi_c(x)$ becomes locked at the value which minimizes $M_c \cos(\sqrt{8}\phi_c)$, leading to $\sqrt{8}\phi_c^a = \gamma_c = \pi \pmod{2\pi}$. If instead m_{cs} is dominant, $\sqrt{8}\phi_c^a = \gamma_c = 0$. Similarly, by minimizing the potential for large positive M'_s one expects $\sqrt{8}\phi_s^a = \gamma_s = \pi$ (in fact M'_s renormalizes to zero when it is positive, but the result $\gamma_s = \pi$ is robust), while for negative M'_s one has instead $\sqrt{8}\phi_s^a = \gamma_s = 0$. This is in agreement with the values obtained in the strong-coupling limit for the BI and the CI.

In the intermediate FI phase the spin gap remains open, and thus the spin Berry phase γ_s is zero, as in the BI. The situation with the charge Berry phase is more delicate: in the thermodynamic limit the inversion symmetry is broken spontaneously, leading to intermediate values of the polarization and also to fractional values of $\sqrt{8}\phi_c^a$, as has been shown in detail for $N=2$.¹⁸ Both quantities are also related to the charge of the fractional excitations of the model.^{10,18} However, for all finite systems, and in particular those of our numerical analysis, the ground state of the FI retains inversion symmetry and $\gamma_c = \pi$ as in the CI phase.

In summary, as for the case $N=2$,¹² the Berry phase vector γ has the value (0, 0) in the BI phase, $(\pi, 0)$ in the FI phase and (π, π) in the CI phase.

Finally, to investigate the possibility of a metallic phase near the charge transition, we have also calculated the Drude weight

$$D_c = \left. \frac{L}{2} \frac{\partial^2 E(L, \Phi)}{\partial \Phi^2} \right|_{\Phi=\Phi_0}, \quad (39)$$

where $E(L, \Phi)$ is the energy of the ground state for a system of length L with (anti-)periodic BCs in the presence of a flux $\Phi hc / (2\pi e)$ threading the ring. For the calculation of $U_L^{c(s)}$ and D_c we have used BCs (or equivalently the choice of Φ_0) corresponding to the closed-shell situation which gives the minimum in the energy as a function of flux.

V. RESULTS

To determine numerically the phase diagram of the AB₂ ($N=3$) and AB₃ chains ($N=4$) we have used both the MCEL,

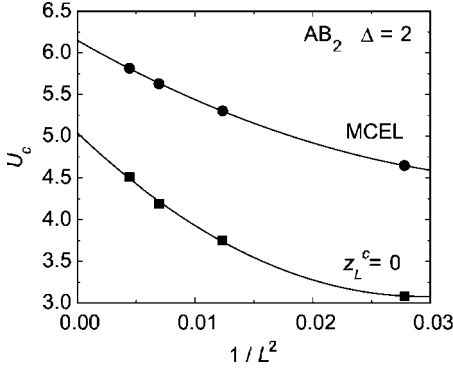


FIG. 3. Critical value of on-site repulsion at the charge transition as a function of $1/L^2$, determined by the MCEL (circles) and by the condition $z_L^c=0$ (squares) for the AB_2 chain with $\Delta=2$.

which corresponds to the jumps in charge and spin Berry phases (above), and the sign of z_L^c , both calculated by exact diagonalization with the Lanczos algorithm. The largest accessible system sizes are then $L=15$ for $N=3$ and $L=16$ for $N=4$, which are sufficient to allow a finite-size scaling analysis of limited accuracy. The two calculational methods should give the same result in the thermodynamic limit [Eq. (37)], although as discussed in the previous section the former is usually more accurate.⁴⁵ However, we have found that for $\Delta \lesssim t$ the level crossings have large finite-size effects, particularly for $N=4$, which limits the comparison of the two techniques. We have extrapolated the transition parameters using a quadratic polynomial in $1/L^2$, a dependence expected from conformal invariance and generally used in the MCEL.^{31,46,47}

Examples of the size dependence of the resulting critical values at the charge (U_c) and spin (U_s) transitions are shown in Figs. 3 and 4, respectively. The unit of energy is chosen as $t=1$. For U_c we have also tested an extrapolation with $1/L^3$ dependence,¹⁹ but the results were significantly inferior and displayed larger errors. For $\Delta > 2$ the error in the extrapolated value of U_c obtained from the condition $z_L^c=0$ is an order of magnitude larger than that obtained from the MCEL. Thus the MCEL may be taken to provide the more accurate results for $\Delta \geq 2$, as expected. For the majority of the parameter range these methods extrapolate acceptably well, and in

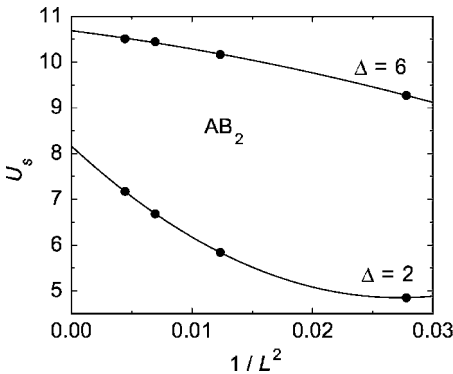


FIG. 4. Critical value of on-site repulsion at the spin transition as a function of $1/L^2$, determined by the MCEL for the AB_2 chain with two values of Δ .

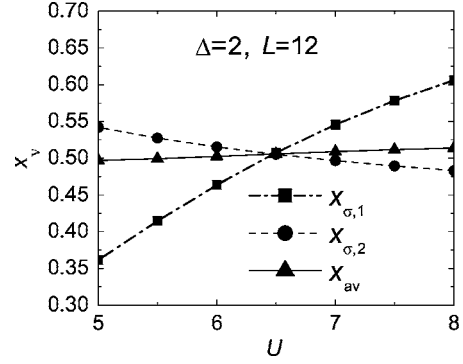


FIG. 5. Scaling dimensions as a function of U for the AB_3 chain with $L=12$ and $\Delta=2$.

a similar manner, towards a fixed value. However, for smaller values of Δ , i.e., in the weak-coupling regime, the quality of the fit deteriorates rapidly for both methods, but particularly for the MCEL. As discussed below, this method becomes unreliable for $N=4$ and $\Delta < 1$.

Figure 4 shows the value of the spin transition (U_s) in the AB_2 chain for different system sizes, obtained using the MCEL. Again the data extrapolate in a satisfactory manner for larger values of Δ , but a comparison of the two curves shows that the quality of the $1/L^2$ fit for the size dependence of U_s also deteriorates with decreasing Δ . A test of the MCEL based on conformal invariance and the renormalization group, and of the Kosterlitz–Thouless character of the spin transition, can be made by calculating the scaling dimensions $x_{\sigma,1}$ of the singlet and $x_{\sigma,2}$ of the triplet excitations.^{31,46} According to the predictions of conformal field theory, the excitation energies should scale according to

$$\Delta E_{\sigma,i} \cong \frac{2\pi v_s}{L} x_{\sigma,i}, \quad (40)$$

where $\Delta E_{\sigma,1}$ ($\Delta E_{\sigma,2}$) is the difference between the energy of the lowest singlet (triplet) state with BCs opposite to the closed-shell situation and the ground-state energy calculated with closed-shell BCs. The spin velocity v_s is calculated from

$$v_s = \frac{E(1, 2\pi/L) - E(0,0)}{2\pi/L}, \quad (41)$$

where $E(S, K)$ is the lowest energy in the sector of total spin S and total wave vector K .

The values of $x_{\sigma,1}$ and $x_{\sigma,2}$ cross at U_s . Their average value $x_{av} = (x_{\sigma,1} + 3x_{\sigma,2})/4$ should be equal to $1/2$ near the crossing, and for $U > U_s$ where the spin gap is closed. Numerical results for the scaling dimensions are shown in Fig. 5. Clearly x_{av} is indeed close to $1/2$, supporting the validity of the MCEL technique for the spin transition. For the reasons discussed in Sec. IV a similar analysis at U_c is less reliable. Systems of larger size may be studied only by the density-matrix renormalization-group technique, which would offer a means of refining the quantitative aspects of the results below, as well as the possibility of investigating the critical behavior at the two transitions.

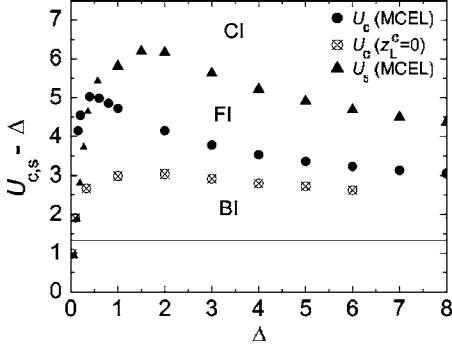


FIG. 6. Phase diagram of the AB₂ chain.

Having demonstrated the application of the numerical methods discussed in Sec. IV, we are now in a position to discuss the phase diagrams of AB_{N-1} chains. In Fig. 6 we show the extrapolated values of $U_c - \Delta$ and $U_s - \Delta$ as functions of Δ for the AB₂ system. The chain lengths used were $L=6, 9, 12$, and 15 . For U_c we compare the results of the MCEL with those obtained from the change of sign of z_L^c [cf. Fig. 3]. The difference between the two methods is significant, particularly for $\Delta \lesssim 1$, where both methods have larger errors. For $\Delta < 0.75$, the points displayed for U_s , and for U_c obtained from z_L^c , were calculated by fixing U and extrapolating the critical value of Δ . In comparison with the results obtained by fixing Δ , this procedure shifts the curves to smaller values of Δ , particularly for the MCEL. For the reasons stated above, at least for $\Delta \geq 2$, we take the MCEL results to be more accurate than those obtained from the change of sign of z_L^c . However, it is clear from Fig. 6 that the two methods agree on a semiquantitative level.

As expected from the strong-coupling analysis of Sec. II, the differences $U_c - \Delta$ and $U_s - \Delta$ are of the order of the hopping t . For comparison, we have drawn two horizontal lines which correspond to the charge and spin transitions obtained with the MCEL for the AB chain (the conventional IHM¹²) for $t \ll U, \Delta$: $U_c - \Delta = 1.33t$ and $U_s - \Delta = 1.91t$. For the AB₂ chain U_c is shifted to larger values, and also the difference $U_s - U_c$ becomes larger for $\Delta \gtrsim t$. Thus while there are no qualitative changes to the phase diagram, the widths of the BI regime and also of the intermediate FI phase increase on passing from AB to AB₂. This is in agreement with the conclusions of the bosonization treatment presented in Sec. III. For $\Delta < t$, the numerical results show a tendency towards a negative difference $U_s - U_c$; this result is difficult to justify on physical grounds, such as those underlying the bosonization treatment, and is in all probability an artifact of finite-size effects, which are of the order of $|U_s - U_c|$ when $U_s - U_c$ is negative.

Figure 7 shows the dependence of the Drude weight D_c and of the expectation value of the localization operator z_L^c as functions of U for $\Delta = 10t$ and for all system sizes studied. The evolution of these quantities with L (D_c decreasing and $|z_L^c|$ increasing) for $U \neq U_c$ indicates that the system is insulating over the entire range of parameters. However, because the system sizes are small one may not exclude metallic behavior at or near the point $U = U_c$. The vanishing value of $|z_L^c|$ at this point and the peak in D_c are consistent with this possibility, but also simply with a larger localization length for

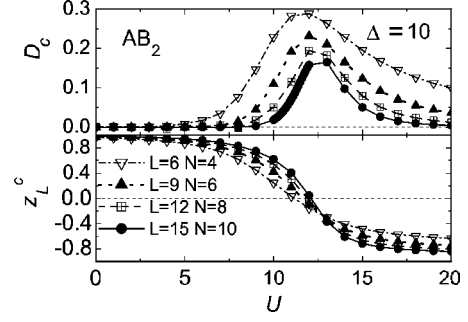


FIG. 7. Drude weight and z_L^c as functions of U in the AB₂ chain with $\Delta = 10$ for a range of system sizes. The critical interaction strength obtained from the MCEL and by extrapolating to the thermodynamic limit is $U_c = 12.94$ for this value of Δ .

$U \sim U_c$. From our theoretical and numerical analyses it is not possible to establish whether or not D_c extrapolates to a finite value, which would indicate metallic behavior in the thermodynamic limit.

In Fig. 8 we show the extrapolated values of $U_c - \Delta$ and $U_s - \Delta$ as functions of Δ for the AB₃ chain. The system sizes used for this case were $L=8, 12$, and 16 , combined with a limited number of runs with $L=20$. For $\Delta < 1$, all of the points displayed except those for U_c obtained within the MCEL were calculated by fixing U and extrapolating the critical value of Δ . Surprisingly, U_c obtained from the MCEL (or the jump in the charge Berry phase) appears to diverge as $\Delta \rightarrow 0$. To be specific, for $U = 50$ (not shown) the extrapolated value of Δ at the transition is $\Delta_c \approx 0.6$, while for $L=8$, $\Delta_c \approx 3$; these results reflect the presence of very large finite-size effects.

This type of behavior is completely inconsistent with the strong-coupling results presented in Sec. II, which show that for any $\Delta > 0$ and $U - \Delta \gtrsim t$, the system is a CI with a charge distribution of the form represented schematically in Fig. 1(b). By contrast, the transition obtained from z_L^c is consistent with the strong-coupling results. This fact, taken in combination with the very large finite-size effects of the MCEL for small Δ , support the conclusion that the level crossing which is followed fails to describe the charge transition for $\Delta \lesssim 1$. This difficulty may be related to the loss of translational symmetry in comparison with the Hubbard model. In fact, in the example of the extended Hubbard model with correlated hopping, where a similar charge transition occurs,^{12,43,44,46} the quantum numbers for the appropriate

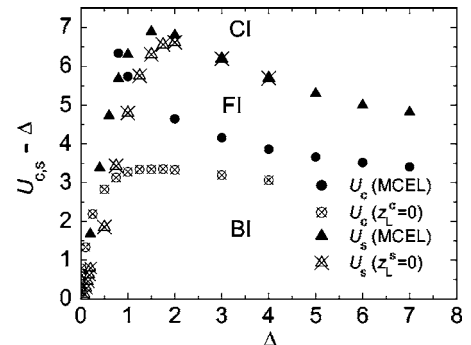


FIG. 8. Phase diagram of the AB₃ chain.

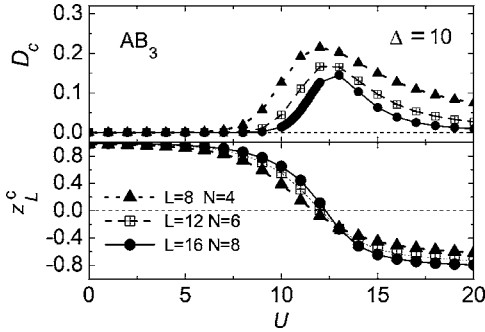


FIG. 9. Drude weight and z_L^c as functions of U in the AB_3 chain with $\Delta=10$ for a range of system sizes. The critical interaction strength obtained from the MCEL and by extrapolating to the thermodynamic limit is $U_c=13.20$ for this value of Δ .

crossing energy levels can be identified from a weak-coupling analysis and correspond to wave vector $K=\pi/a_0$.⁴⁶ When the one-site translational symmetry is lost, this wave vector is mixed with others and the Lanczos method, which captures the lowest eigenstate for the corresponding wave vector in the reduced Brillouin zone, no longer follows necessarily the correct excitation in the weakly coupled case. This problem arises also in the extended IHM.¹²

We proceed by disregarding the points obtained for the charge transition with the MCEL for $\Delta \leq 1$, and in this regime adopt the values obtained from z_L^c . The phase diagram of the AB_3 chain (Fig. 8) is very similar to that of AB_2 . Only at the quantitative level is there a moderate shift of U_c and U_s to still larger values and a small increase in the width of the region occupied by the FI phase. In Fig. 8 we show also the values of U_s for the spin transition obtained from the condition $z_L^s=0$. These are in very close coincidence with the results obtained from the MCEL for $\Delta \geq 2$; for small Δ both methods are again plagued by large finite-size effects, but the discrepancy between the extrapolated values is significantly smaller than in the case of the charge transition.

Finally, Fig. 9 displays the dependence of D_c and z_L^c on U in an AB_3 chain with $\Delta=10t$ for several system sizes. The results are qualitatively and quantitatively very similar to those obtained for the AB_2 system (Fig. 7). At $U > U_c$ some indications of a smaller gap and longer localization length might have been expected as the size of the unit cell N increases, as suggested by the results of Sec. II, but in this respect no significant differences are found between the AB_2 and AB_3 chains investigated here.

VI. SUMMARY AND DISCUSSION

We have performed a systematic analysis of the generalized ionic Hubbard model (IHM) in one dimension. Motivated by the complex behavior emerging in the AB chain, where the commensurate filling ensures a dominant role for Umklapp scattering terms, we have investigated the phase diagrams for AB_{N-1} chains with unit cell size N and filling $1/N$. We have employed analytical considerations in both weak- and strong-coupling limits, and sophisticated numerical techniques based on Lanczos exact diagonalization, applying these specifically to the cases $N=3$ and $N=4$.

Despite the absence of direct Umklapp terms away from $N=2$, we find that the qualitative features of the AB_{N-1} phase diagram are essentially identical to those of the conventional IHM. The generalized model always possesses three phases as a function increasing values of U : a band insulator (BI) for small U/Δ , a correlated insulator (CI) for large U/Δ which is a form of Mott insulator, and between these an intermediate ferroelectric insulator (FI) with spontaneous breaking of inversion symmetry and fractional excitations. The generic nature of the phase diagram is explained within a bosonization analysis by the emergence of higher-order interaction terms related to the charge-density modulation caused by the ionic term.

The general similarity of all the models in this class masks some important differences. Qualitatively, the CI phase for large U is not strictly a Mott insulator because the number of particles is less than the number of sites. As a quantitative consequence, the localization length is therefore larger than one lattice parameter and the gap is much smaller than in the conventional ($N=2$) IHM. In the latter, for large U the gap is of order $U-\Delta$, whereas for $N>2$ it is given by Eq. (2) and vanishes for $\Delta=0$; we note here that in all cases ($N=2$ and $N>2$) the large- U phase, which for $N>2$ and $\Delta=0$ is a Luttinger liquid, becomes a CI for any nonzero value of Δ . More generally, the relatively weaker Umklapp terms result in larger values of U being required to compete with the ionic term Δ , which favors the BI phase, and thus the FI and CI phase boundaries are pushed to larger U with increasing N ; both BI and FI regimes are broadened.

We have implemented the numerical calculation of a number of characteristic quantities which provide valuable insight into the properties of the ground and excited states. For the two phase boundaries we have employed the method of crossing excitation levels (MCELs), which is equivalent to following discontinuous steps in the charge and spin Berry phases, quantities which signal the presence of a transition even on a small system. This calculation is compared with the results obtained from the vanishing of the expectation value of the displacement operators, which is found to be a less accurate but sometimes more reliable technique. We have also computed the Drude weight with a view to testing the possible metallic nature of the system at the phase boundaries between the insulating phases.

While the numerical analysis serves as a useful test of these techniques, and allows us to make certain powerful qualitative statements, the results are also subject to strong finite-size effects. In particular, the MCEL has significantly larger finite-size effects for $N>2$ than at $N=2$, due probably to the much smaller gap in the CI phase and the relatively lower translational symmetry. Indeed, at the charge transition for $\Delta < t$ the phase of z_L^c gives more reliable information. However, even with the restricted system sizes accessible in our study, the majority of the results obtained in Sec. V can be said to be of semiquantitative accuracy. We comment that further studies on systems of larger size are possible using the density-matrix renormalization-group technique: with the aid of the quantities we have defined and analyzed in Secs. IV and V, such calculations might confirm our findings with greater accuracy, establish more precisely the boundary of the charge transition, and possibly also permit the analysis of critical behavior at the two transitions.

In the same way that the AB chain has for many years been of interest in the context of quasi-one-dimensional organic MX complexes, our considerations concerning the AB_2 chain are expected to be relevant for the properties of MMX chains. These are halogen-bridged binuclear metal chains such as $R_4[Pt_2(P_2O_5H_2)_4X \cdot nH_2O]$, on which experimental studies would be welcomed. We comment that the greater extent in parameter space of the FI phase for $N > 2$ systems may even be important for technological applications. Finally, with regard to the possible metallic properties of AB_{N-1} systems, we have found that despite being at fillings $1/N$ away from the half-filled situation, these remain insulating for all parameter regimes other than $\Delta=0$, as a conse-

quence of the commensurate nature of their electron number. Only at the charge transition do we obtain evidence from the Drude weight and from the charge localization operator of a possible metallic point in the phase diagram.

ACKNOWLEDGMENTS

This work was sponsored by PICT 03-12742 of ANPCyT. M.E.T. and A.A.A. are partially supported by CONICET. G.I.J. acknowledges support through SCOPES Grant No. 7GEPJ62379 of the Swiss NSF, and the generous hospitality of the MPI-PKS Dresden, where part of this work was performed.

-
- ¹J. Hubbard and J. B. Torrance, Phys. Rev. Lett. **47**, 1750 (1981).
²N. Nagaosa and J. Takimoto, J. Phys. Soc. Jpn. **55**, 2735 (1986).
³M. H. Lemée-Cailleau, M. Le Cointe, H. Cailleau, T. Luty, F. Moussa, J. Roos, D. Brinkman, B. Toudic, C. Ayache, and N. Karl, Phys. Rev. Lett. **79**, 1690 (1997).
⁴S. Horiuchi, Y. Okimoto, R. Kumai, and Y. Tokura, J. Phys. Soc. Jpn. **69**, 1302 (2000).
⁵S. Ishihara, T. Egami, and M. Tachiki, Science **261**, 1307 (1993); Phys. Rev. B **49**, 8944 (1994).
⁶R. Resta and S. Sorella, Phys. Rev. Lett. **74**, 4738 (1995).
⁷G. Ortiz, P. Ordejón, R. M. Martin, and G. Chiappe, Phys. Rev. B **54**, 13515 (1996), and references therein.
⁸R. Resta and S. Sorella, Phys. Rev. Lett. **82**, 370 (1999).
⁹N. Gidopoulos, S. Sorella, and E. Tosatti, Eur. Phys. J. B **14**, 217 (2000).
¹⁰M. Fabrizio, A. O. Gogolin, and A. A. Nersesyan, Phys. Rev. Lett. **83**, 2014 (1999).
¹¹M. Fabrizio, A. O. Gogolin, and A. A. Nersesyan, Nucl. Phys. B **580**, 647 (2000).
¹²M. E. Torio, A. A. Aligia, and H. A. Ceccatto, Phys. Rev. B **64**, 121105(R) (2001).
¹³Y. Z. Zhang, C. Q. Wu, and H. Q. Lin, Phys. Rev. B **67**, 205109(R) (2003).
¹⁴A. P. Kampf, M. Sekania, G. I. Japaridze, and P. Brune, J. Phys. C **15**, 5895 (2003).
¹⁵A. A. Aligia, Phys. Rev. B **69**, 041101(R) (2004).
¹⁶S. R. Manmana, V. Meden, R. M. Noack, and K. Schönhammer, Phys. Rev. B **70**, 155115 (2004).
¹⁷C. D. Batista and A. A. Aligia, Phys. Rev. Lett. **92**, 246405 (2004).
¹⁸A. A. Aligia and C. D. Batista, Phys. Rev. B **71**, 125110 (2005).
¹⁹H. Otsuka and M. Nakamura, Phys. Rev. B **71**, 155105 (2005).
²⁰A. A. Aligia, K. Hallberg, B. Normand, and A. P. Kampf, Phys. Rev. Lett. **93**, 076801 (2004).
²¹T. Wilkens and R. M. Martin, Phys. Rev. B **63**, 235108 (2001).
²²S. Yamamoto, Phys. Rev. B **64**, 140102(R) (2001).
²³E. H. Lieb and F. Y. Wu, Phys. Rev. Lett. **20**, 1445 (1968).
²⁴H. J. Schulz, Phys. Rev. Lett. **64**, 2831 (1990).
²⁵F. H. L. Essler, V. E. Korepin, and K. Schoutens, Phys. Rev. Lett. **67**, 3848 (1991).
²⁶W. Caspers and P. Iiske, Physica A **157**, 1033 (1989).
²⁷A. Schadschneider, Phys. Rev. B **51**, 10386 (1995).
²⁸M. Ogata and H. Shiba, Phys. Rev. B **41**, 2326 (1990).
²⁹T. Pruschke and H. Shiba, Phys. Rev. B **44**, 205 (1991).
³⁰K. Penc and F. Mila, Phys. Rev. B **50**, 11429 (1994).
³¹K. Nomura and K. Okamoto, J. Phys. A **27**, 5773 (1994).
³²A. O. Gogolin, A. A. Nersesyan, and A. M. Tsvelik, *Bosonization and Strongly Correlated Systems* (Cambridge University Press, Cambridge, 1998).
³³J. Voit, Rep. Prog. Phys. **58**, 977 (1995).
³⁴D. Sénéchal, in *Theoretical Methods for Strongly Correlated Electrons*, edited by D. Sénéchal, A.-M. Tremblay, and C. Bourbonnais (Springer, Berlin, 2004).
³⁵If the fermion fields are defined without the Klein operators $\kappa_{\pm,s}^\dagger$ in Eq. (10), different bosonized expressions are obtained for several quantities, which correspond to a shift by $\pi/\sqrt{8}$ in the field ϕ_c . However, all physical observables remain unchanged. The convention chosen here leads to analogous forms for \mathcal{H}_c and \mathcal{H}_s , and for z_L^c and z_L^s , and has been used for $N=2$ by one of the authors.¹⁸ The alternative convention was used by Fabrizio and co-workers.
³⁶G. Bedürftig, B. Brendel, H. Frahm, and R. M. Noack, Phys. Rev. B **58**, 10225 (1998).
³⁷J. Voit, Phys. Rev. B **45**, 4027 (1992).
³⁸G. I. Japaridze, Phys. Lett. A **201**, 239 (1995); G. I. Japaridze and A. P. Kampf, Phys. Rev. B **59**, 12822 (1999).
³⁹R. Resta, Rev. Mod. Phys. **66**, 899 (1994).
⁴⁰G. Ortiz and R. M. Martin, Phys. Rev. B **49**, 14202 (1994).
⁴¹M. E. Torio, A. A. Aligia, K. Hallberg, and H. A. Ceccatto, Phys. Rev. B **62**, 6991 (2000).
⁴²A. A. Aligia, Europhys. Lett. **45**, 411 (1999).
⁴³A. A. Aligia and L. Arrachea, Phys. Rev. B **60**, 15332 (1999), and references therein.
⁴⁴A. A. Aligia, K. Hallberg, C. D. Batista, and G. Ortiz, Phys. Rev. B **61**, 7883 (2000).
⁴⁵A. A. Aligia and G. Ortiz, Phys. Rev. Lett. **82**, 2560 (1999).
⁴⁶M. Nakamura, J. Phys. Soc. Jpn. **68**, 3123 (1999); Phys. Rev. B **61**, 16377 (2000).
⁴⁷R. D. Somma and A. A. Aligia, Phys. Rev. B **64**, 024410 (2001).
⁴⁸P. Sindzingre, J.-B. Fouet, and C. Lhuillier, Phys. Rev. B **66**, 174424 (2002).
⁴⁹N. Shannon, G. Misguich, and K. Penc, Phys. Rev. B **69**, 220403(R) (2004).
⁵⁰G. Ortiz and A. A. Aligia, Phys. Status Solidi B **220**, 737 (2000).